RESEARCH ARTICLE

Physical properties and seismic structure of Izu-Bonin-Mariana fore-arc crust: Results from IODP Expedition 352 and comparison with oceanic crust

G. L. Christeson[1], S. Morgan[2], S. Kodaira [ID][3], M. Yamashita[3], R. R. Almeev[4], K. Michibayashi [ID][5], T. Sakuyama[6], E. C. Ferré [ID][7], and W. Kurz [ID][8]

[1]University of Texas Institute for Geophysics, Jackson School of Geosciences, Austin, Texas, USA, [2]Department of Geology, University of Leicester, Leicester, UK, [3]JAMSTEC Japan Agency for Marine-Earth Science and Technology, Yokosuka, Japan, [4]Leibniz Universität Hannover, Institute of Mineralogy, Hannover, Germany, [5]Institute of Geosciences, Shizuoka University, Shizuoka, Japan, [6]Department of Geosciences, Osaka City University, Osaka, Japan, [7]Department of Geology, Southern Illinois University, Carbondale, Illinois, USA, [8]Institute of Earth Sciences, NAWI Graz Geocenter, University of Graz, Graz, Austria

Abstract Most of the well-preserved ophiolite complexes are believed to form in suprasubduction zone (SSZ) settings. We compare physical properties and seismic structure of SSZ crust at the Izu-Bonin-Mariana (IBM) fore arc with oceanic crust drilled at Holes 504B and 1256D to evaluate the similarities of SSZ and oceanic crust. Expedition 352 basement consists of fore-arc basalt (FAB) and boninite lavas and dikes. *P*-wave sonic log velocities are substantially lower for the IBM fore arc (mean values 3.1–3.4 km/s) compared to Holes 504B and 1256D (mean values 5.0–5.2 km/s) at depths of 0–300 m below the sediment-basement interface. For similar porosities, lower *P*-wave sonic log velocities are observed at the IBM fore arc than at Holes 504B and 1256D. We use a theoretical asperity compression model to calculate the fractional area of asperity contact A_f across cracks. A_f values are 0.021–0.025 at the IBM fore arc and 0.074–0.080 at Holes 504B and 1256D for similar depth intervals (0–300 m within basement). The A_f values indicate more open (but not necessarily wider) cracks in the IBM fore arc than for the oceanic crust at Holes 504B and 1256D, which is consistent with observations of fracturing and alteration at the Expedition 352 sites. Seismic refraction data constrain a crustal thickness of 10–15 km along the IBM fore arc. Implications and inferences are that crust-composing ophiolites formed at SSZ settings could be thick and modified after accretion, and these processes should be considered when using ophiolites as an analog for oceanic crust.

1. Introduction

Ophiolites are often used as an analog for oceanic crust because their lithological sequences (lavas, sheeted dikes, gabbros, and ultramafics) are similar to those observed at oceanic drill sites [e.g., *Moores and Vine*, 1971; *Anonymous*, 1972]. However, most ophiolites are thought to have formed in a suprasubduction zone (SSZ) setting rather than at mid-ocean ridges [e.g., *Miyashiro*, 1973; *Pearce et al.*, 1984]. Hence, it is important to constrain how representative SSZ crust is to normal oceanic crust. Our focus in this study is on the geophysical properties of SSZ and oceanic crust.

One of the type localities for studying SSZ crust is the Izu-Bonin-Mariana (IBM) system (Figure 1a). IBM subduction initiated ∼52 Ma when a change in plate motion resulted in compression between the Pacific and Philippine Sea plates [*Hilde et al.*, 1977; *Stern and Bloomer*, 1992; *Ishizuka et al.*, 2011; *Reagan et al.*, 2013]. Soon after subduction initiation, spreading commenced in the fore arc, producing mid-ocean ridge basalt (MORB)-like tholeiitic basalts which have been termed "fore-arc basalts" (FAB) [*Reagan et al.*, 2010]. With continuing subduction, erupted lavas evolved to boninites, transitional lavas, and eventually traditional arc volcanics [*Stern and Bloomer*, 1992; *Ishizuka et al.*, 2011; *Reagan et al.*, 2013]. A seismic refraction survey in the Izu-Bonin fore arc found thin arc crust that is remarkably similar in thickness to typical oceanic crust, and it has been argued that this crust is an ophiolite in the process of being obducted [*Kodaira et al.*, 2010].
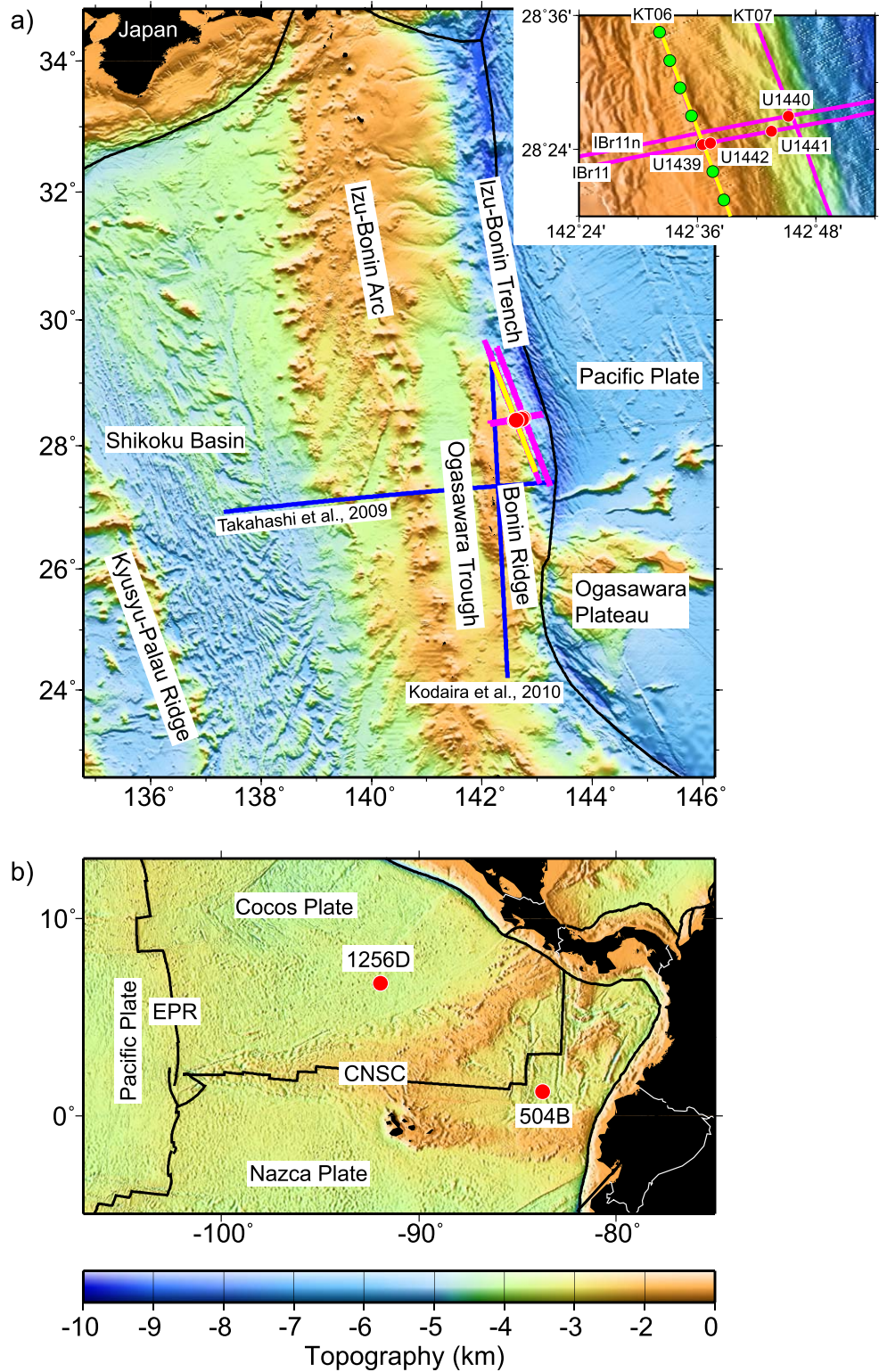
Figure 1. Location maps showing tectonic setting of (a) IODP Expedition 352 sites in the Izu-Bonin system; (b) DSDP/ODP Hole 504B and ODP/IODP Hole 1256D in the eastern Pacific. Red circles mark locations of drill sites; black lines mark plate boundaries. Seismic site survey data for IODP Expedition 352 are shown with magenta (MCS profiles) and yellow (coincident seismic refraction profile) lines, and seismic refraction profiles of *Takahashi et al.* [2009] and *Kodaira et al.* [2010] are shown with blue lines. Background is topography from the global multi-resolution topography synthesis [*Ryan et al.*, 2009]. CNSC: Cocos-Nazca Spreading Center; EPR: East Pacific Rise. Inset shows close-up of the IODP Expedition 352 drill sites and seismic site survey data; ocean bottom seismometer positions are displayed with green circles.

Recent drilling at the IBM fore arc during International Ocean Discovery Program (IODP) Expedition 352 penetrated a total of more than 1 km of basement from four different sites [*Expedition 352 Scientists*, 2014]. In this study we compare physical properties, logging, and seismic site survey data from these sites to the equivalent measurements from Holes 504B and 1256D in the East Pacific Ocean (Figure 1b) to evaluate how representative SSZ crust is compared to normal oceanic crust. We then consider what implications this comparison has for using ophiolites as analogs for oceanic crust.

2. Drill Sites

IODP Expedition 352 drilled seven holes across four sites in the Izu-Bonin fore arc at the northeastern edge of the Bonin Ridge (Figure 1a). Here we study Holes U1439C, U1440B, U1441A, and U1442A which cored 362, 268, 123, and 447 m of basement rocks, respectively [*Expedition 352 Scientists*, 2014]. At Holes U1440B and U1441A, located closest to the trench, basement consists of fore-arc basalts, with ~145 m of lavas overlying a ~70 m thick transition zone of lavas and dikes, which in turn overlies a ~55 m thick sheeted dike unit or sill complex at the bottom of Hole U1440B [*Expedition 352 Scientists*, 2014]. At Holes U1439C and U1442A, located further west from the trench, basement consists of boninite group lavas, with 28 m of a dike or sill complex at the base of Hole U1439C [*Expedition 352 Scientists*, 2014]. Logging was carried out at Holes U1439C, U1440B, and U1442A, although hole conditions precluded the logging tools reaching the bottom of any of these holes [*Expedition 352 Scientists*, 2014].

Hole 504B is located in ~5.9 Ma intermediate spreading rate crust formed at the Cocos-Nazca spreading center (Figure 1b) [e.g., *Anderson et al.*, 1982; *Becker et al.*, 1989; *Alt et al.*, 1993]. Multiple drilling legs penetrated 1836 m into basement, consisting of 571 m of lavas, 209 m of a lava-dike transition zone, and 1056 m of a sheeted dike complex [*Alt et al.*, 1993]. Logging was carried out over the entire length of basement [*Alt et al.*, 1993].

Hole 1256D is located in ~15 Ma superfast spreading crust generated at the East Pacific Rise (Figure 1b) [*Shipboard Scientific Party*, 2003; *Expedition 309 and 312 Scientists*, 2006; *Wilson et al.*, 2006]. Four drilling legs penetrated 1272 m into basement, consisting of 754 m of lavas and flows, 57 m of a lava-dike transition zone, 346 m of a sheeted dike complex, and 115 m of a plutonic section with gabbros and dike screens [*Expedition 335 Scientists*, 2011]. Logging was carried out over almost the entire length of basement [*Expedition 309 and 312 Scientists*, 2006; *Expedition 335 Scientists*, 2011].

3. Measurements and Data Analysis

3.1. Discrete Sample Measurements

During Expedition 352, compressional seismic velocity, density, and porosity measurements were made at room temperature and pressure on discrete cube samples (8 cm^3) taken approximately every 3 m of recovered basement core for all sites [*Expedition 352 Scientists*, 2014]. Figure 2 compares compressional seismic velocity with porosity and density for all measurements, with boninite suite and fore-arc basalt suite samples plotted with red and blue symbols, respectively. Also plotted are similar measurements for Hole 504B (cyan symbols) [*Karato et al.*, 1983] and Hole 1256D (green symbols) [*Wilson et al.*, 2003; *Expedition 309 Scientists*, 2005] for samples from the upper 300 m of basement, which is the average basement penetration depth for the Expedition 352 sites.

3.2. Logging Measurements

A series of in situ borehole measurements was acquired during Expedition 352 and at Holes 504B and 1256D, including sonic velocity, resistivity, bulk density, and gamma ray [e.g., *Alt et al.*, 1993; *Expedition 309 and 312 Scientists*, 2006; *Expedition 335 Scientists*, 2011; *Expedition 352 Scientists*, 2014]. Porosity in oceanic basement can be estimated from resistivity using Archie's law [*Archie*, 1942] and the method of *Becker et al.* [1982]. Figure 3 displays compressional velocity, porosity, density, and gamma ray logs for the upper 300 m of basement for all sites in our study; because of hole conditions, logging tools did not advance deeper than 300 m into basement at the Expedition 352 sites [*Expedition 352 Scientists*, 2014]. Figure 4 compares compressional seismic velocities with porosity and density for log measurements at basement depths of 25–300 m (values from 0 to 25 m are excluded because of the high variability observed in porosity values).
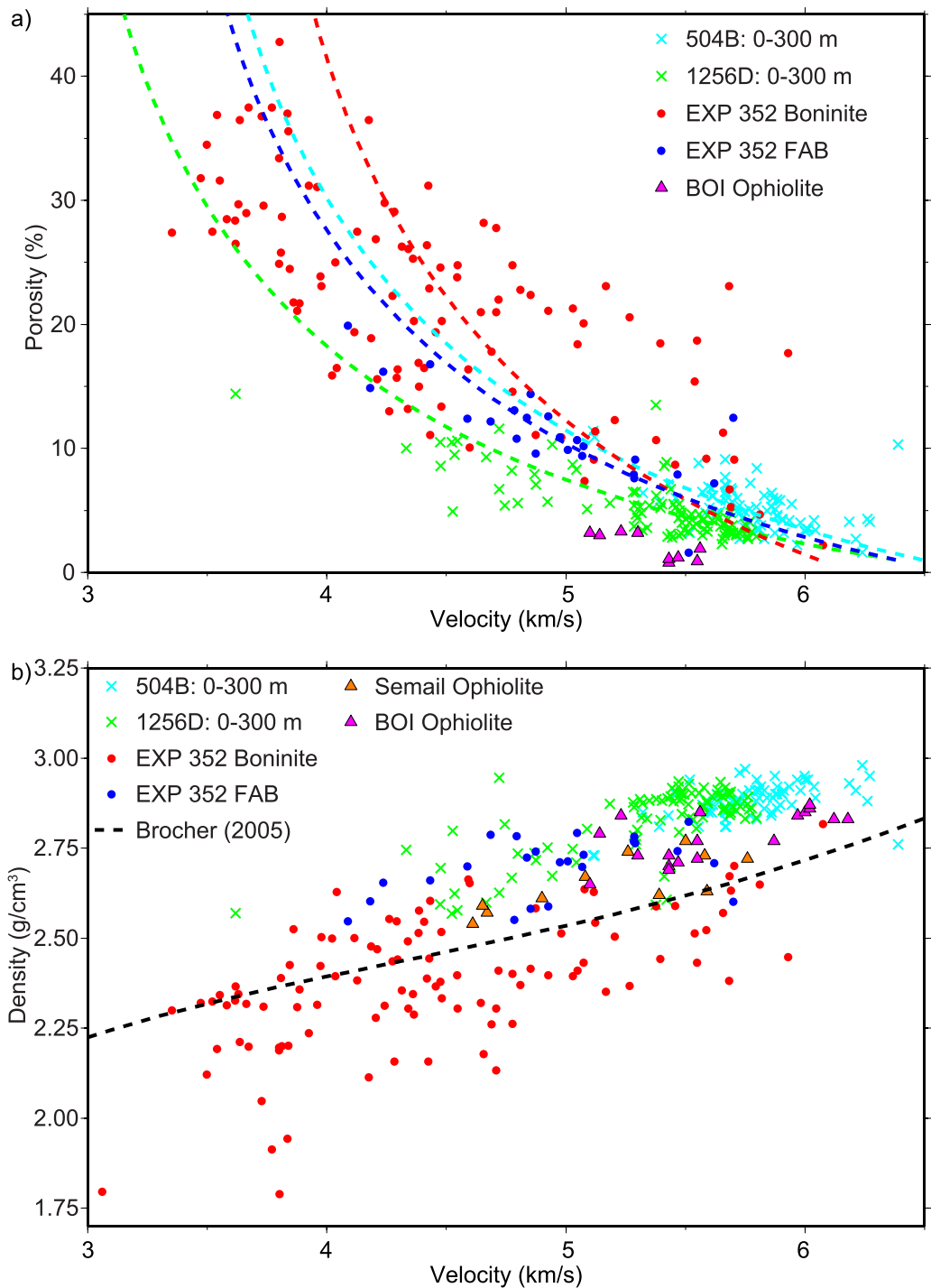
Figure 2. Scatterplots of velocity compared to (a) porosity and (b) density for discrete samples from IODP Expedition 352 Holes U1439C and U1442A (boninite suite), Holes U1440B and U1441A (fore-arc basalt (FAB) suite), oceanic crust Holes 504B and 1256D, and the Semail [*Christensen and Smewing*, 1981] and Bay of Islands (BOI) [*Salisbury and Christensen*, 1978; *Christensen and Salisbury*, 1982] ophiolites. For Holes 504B and 1256D measurements are only plotted for samples from the upper 300 m of basement. The ophiolite sample measurements were made at pressures of 0.06–0.08 GPa; 0.18 km/s has been subtracted from the velocity values for comparison with the other samples which were measured at ambient pressure. Colored dashed lines in the top figure plot the calculated relationships between porosities and velocities using the asperity compression model of *Carlson* [2014b]. Black dashed line in the bottom figure plots the global relationship between velocity and density from *Brocher* [2005].

3.3. Crack Morphology Models

Carlson [2014b] presents a theoretical asperity compression model that provides a good fit to log data from Holes 504B and 1256D. In the model the key parameter is A_f, the fractional area of asperity contact across
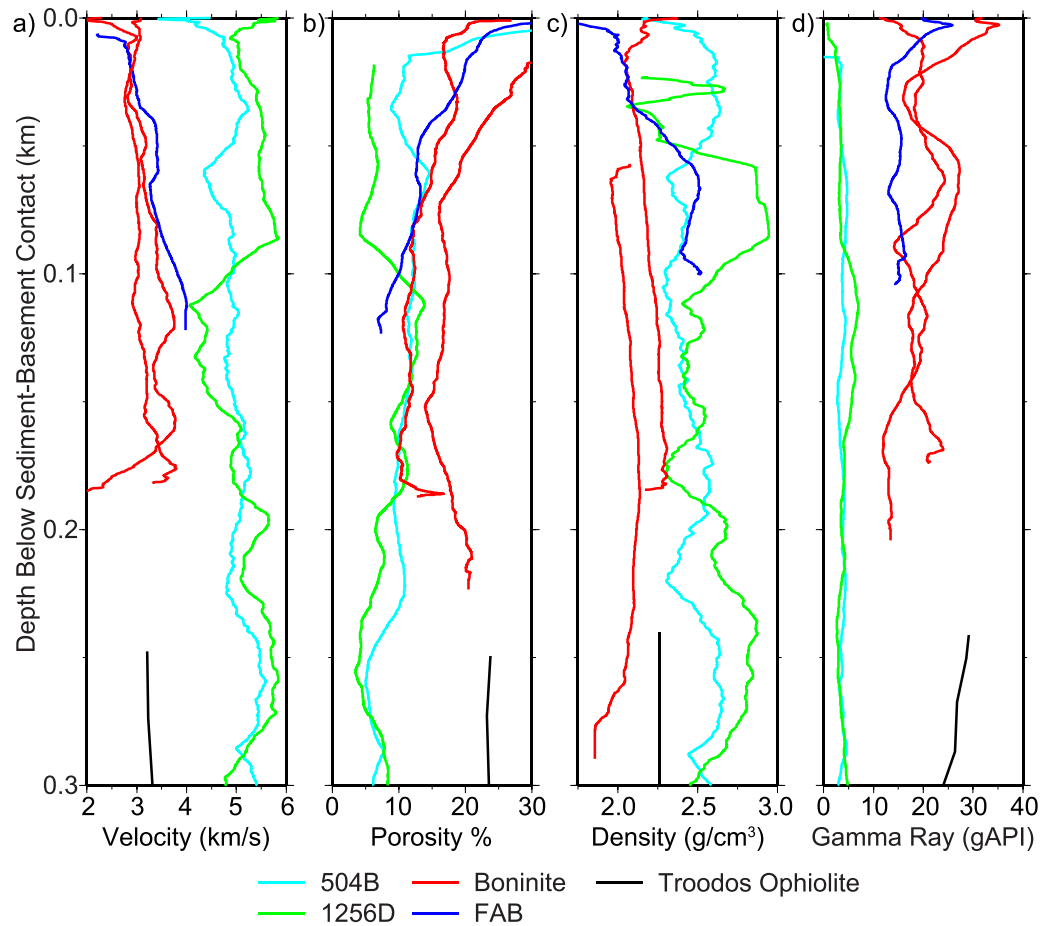
Figure 3. Logs in the upper 300 m of basement for IODP Expedition 352 Holes U1439C and U1442A (boninite suite), Hole U1440B (fore-arc basalt (FAB) suite), and oceanic crust Holes 504B and 1256D; logs have a 25 m smoothing window. Sonic logs for Holes 504B and 1256D are from *Guerin et al.* [2008], while all other logs are from online database managed by Lamont-Doherty Earth Observatory. Plotted in black are the average formation properties versus depth derived from logs in the Troodos ophiolite [*Salisbury et al.*, 1989]. (a) P-wave sonic; (b) porosity calculated from resistivity using the method of *Becker et al.* [1982] for ocean drilling logs and calculated from the density log and measured grain densities for the Troodos ophiolite; (c) density; (d) gamma ray reported in gAPI units for ocean drilling logs and API units for the Troodos ophiolite.

the cracks [*Carlson*, 2014b]. We use the following equations from *Carlson* [2014a] and *Carlson* [2014b] to calculate A_f values for our study.

First we calculate bulk density of the rock, ρ_r

$$\rho_r = \phi \rho_f + (1-\phi)\rho_g, \tag{1}$$

where ρ_g is the grain density, ρ_f is the density of the pore fluid, and ϕ is porosity.

We calculate the P-wave moduli, M_{ri}

$$M_{ri} = \rho_{ri} v_{ri}^2, \tag{2}$$

where ρ_r values are from equation (1) and v_r is P-wave velocity.
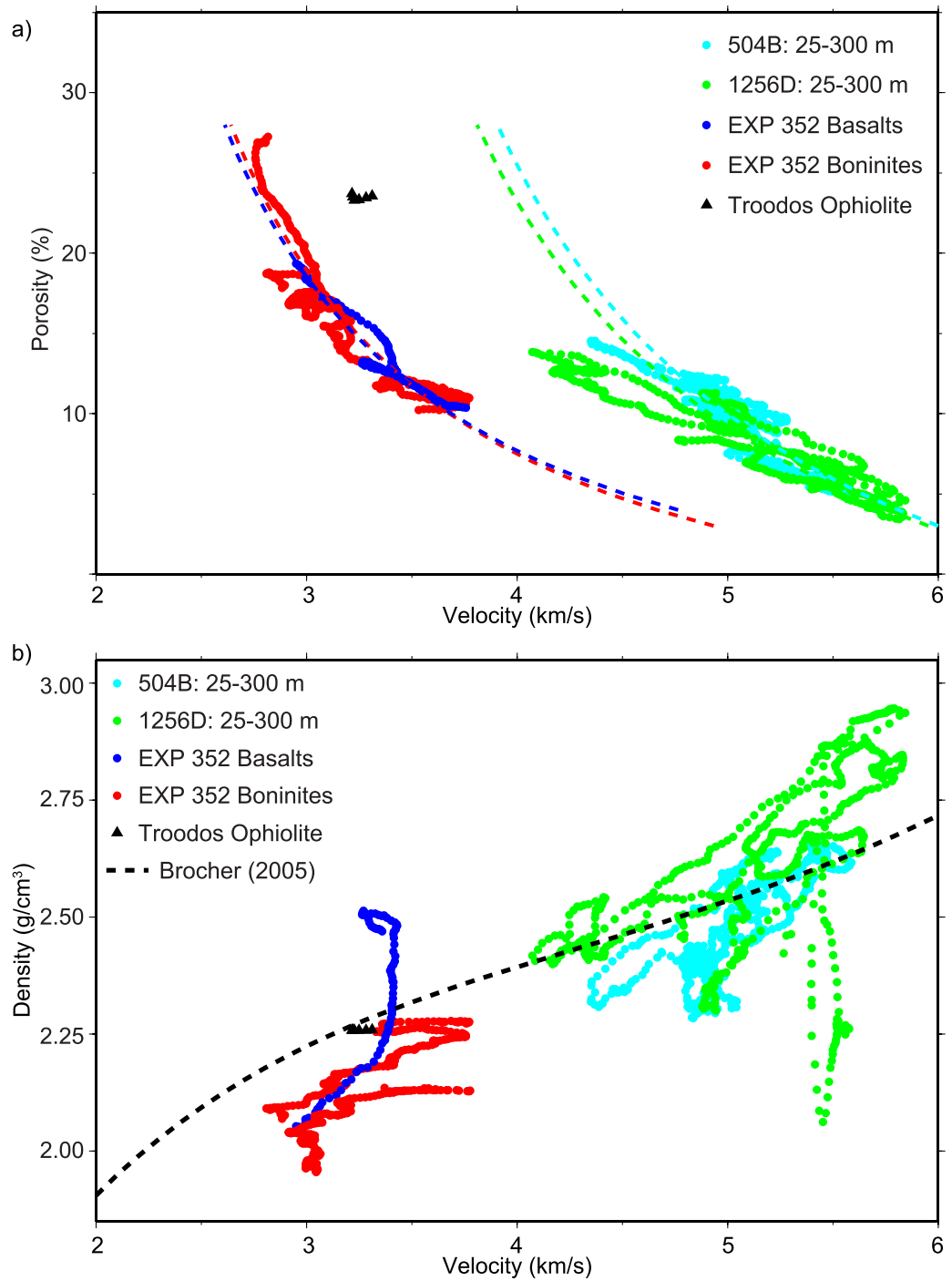
We calculate the P-wave modulus of the grains, M_g, using an empirical relationship [*Carlson*, 2014a],

$$M_g = -309 + 0.15\rho_g. \tag{3}$$

We calculate the best fitting value of M_{cr} to the Reuss-average model for M_r

$$\frac{1}{M_r} = \frac{\phi}{M_{cr}} + \frac{(1-\phi)}{M_g}, \tag{4}$$

where M_r is the P-wave modulus of the rock and M_{cr} is the crack modulus.

Figure 4. Scatterplots of velocity compared to (a) porosity and (b) density for logging measurements from IODP Expedition 352 Holes U1439C and U1442A (boninite suite), Hole U1440B (fore-arc basalt (FAB) suite), and oceanic crust Holes 504B and 1256D. For all sites measurements are only presented for the upper 25–300 m of basement. Also plotted are the same parameters from the average formation properties in the upper 300 m from the Troodos ophiolite [*Salisbury et al.*, 1989]. Colored dashed lines in the top figure plot the calculated relationships between porosities and velocities using the asperity compression model of *Carlson* [2014b]. Black dashed line in the bottom figure plots the global relationship between velocity and density from *Brocher* [2005].

Finally, we calculate A_f

$$A_f = \frac{M_{cr} - M_f}{M_g - M_f},$$

(5)

where M_f is the fluid modulus.

Table 1. Asperity Compression Model Parameters and Standard Deviations

Parameter	EXP352 Basalts	EXP352 Boninites	Hole 504B Basalts	Hole 1256D Basalts
Fluid density, ρ_f (kg/m^3)	1,023	1,023	1,023	1,023
Fluid modulus, M_f (MPa)	2,440	2,440	2,440	2,440
Grain density, ρ_g (kg/m^3)	2,911 ± 64	2,770 ± 108	2,950 ± 0.066	2,950 ± 0.066
Grain modulus, M_g (MPa)	127,719 ± 9647	106,490 ± 16,254	133,437 ± 9,877	133,437 ± 9,877
Crack modulus (logs), M_{cr} (MPa)	5,042 ± 204	4,993 ± 385	12,920 ± 1,101	12,173 ± 1,803
Area of contact (logs), A_f	0.021 ± 0.002	0.025 ± 0.004	0.080 ± 0.008	0.074 ± 0.014
Crack modulus (discrete), M_{cr} (MPa)	13,461 ± 3,490	16,542 ± 7,337	14,278 ± 430	10,182 ± 2,408
Area of contact (discrete), A_f	0.088 ± 0.028	0.136 ± 0.071	0.087 ± 0.031	0.061 ± 0.019

Table 1 summarizes the model parameters. Fluid density and fluid modulus follow *Carlson* [2014b], grain density is the average of discrete sample measurements at depths 0–300 m below basement, and grain modulus, crack modulus, and area of contact are from equations (3)–(5).

### 3.4. Seismic Reflection Images

Multichannel seismic (MCS) data are available for Holes 504B and 1256D and all Expedition 352 sites. MCS data in the IBM fore arc were acquired in 2011 and 2013 with a 118 L air gun array at a shot interval of 50 m, and were recorded by a 444-channel streamer cable 5550 m long. MCS data across Hole 1256D were acquired in 1999 with a 49 L air gun array shot at a shot interval of 37.5 m, and were recorded by a 480-channel streamer cable 6000 m long [*Hallenborg et al.*, 2003]. MCS data across Hole 504B were acquired in 1994 with a 49 L air gun array shot at a nominal shot interval of 33 m and were recorded by a 160-channel streamer cable 4000 m long [*Kent et al.*, 1996, 1997]. All data were processed with the same sequence, which included a band-pass filter, deconvolution, trace regularization, velocity analysis, radon transform multiple attenuation, and 2-D Kirchhoff prestack time migration.

All images were converted to depth with velocities of 1500 m/s for the water column and 1700 m/s for sediments; sediment velocities were chosen based on mean interval velocities from the semblance velocity analyses (which happened to be similar for the IBM, Hole 504B, and Hole 1256D data). A velocity function, based on appropriate seismic refraction profiles, was hung below the seafloor-basement contact. For the IBM sites, the crustal velocity function is from seismic refraction profile KT06 at the location of Hole U1439C (section 3.5). Seismic refraction studies constrain similar velocity functions for Holes 504B and 1256D [*Detrick et al.*, 1998; *Expedition 309 Scientists*, 2005], and thus the identical velocity function was used for depth conversion at both sites (the "northeast" velocity function of Hole 1256D [*Expedition 309 Scientists*, 2005]; section 4.5). Images across all sites, focusing on the upper crust, are displayed in Figure 5 (IBM sites U1439, U1440, and U1442) and Figure 6 (Holes 1256D and 504B).

3.5. Seismic Refraction Data

Trench-parallel seismic refraction profile KT06 crosses Site U1439 in the IBM fore arc (Figure 1). Data were acquired in 2011 using a 118 L air gun array at a shot interval of 200 m, with shots recorded by 43 ocean bottom seismometers (OBSs) at 5 km spacing. The profile is 273 km long, with OBSs positioned at distances 41–251 km from the northernmost shot. Sample record sections are displayed in Figure 7. Crustal refractions (*Pg*) are observed on all instruments up to source-receiver offsets of 30–45 km (Figure 7). Moho reflections (*PmP*) are observed on 26 of the OBSs (e.g., Figures 7a–7c), while mantle refractions (*Pn*) are only identified on eight instruments (e.g., Figure 7d). Other coherent secondary arrivals are observed on some record sections, but have little consistency in time or slope between instruments, and were not included in the analysis; these arrivals are likely associated with reflections from the subducting slab.

We use the iterative tomographic inversion method of *Van Avendonk et al.* [2004] to build a velocity model from the data. The model includes three layers: water, crust, and mantle. Travel time picks were made on the vertical channel; phase identification was refined by overlying travel time curves on the record sections as the inversion proceeded. The final model used 2848 *Pg* picks, 472 *PmP* picks, and 83 *Pn* picks, and achieved a chi-squared value of 1.1 with RMS values between observed and calculated travel times of 69, 67, and 86 ms for the *Pg*, *PmP*, and *Pn* phases, respectively. Raypaths and travel time fits are displayed in Figure 8 for the different phases. Ray coverage is good in the upper and middle crust (Figure 8a). Moho reflections constrain crustal thickness over a lateral
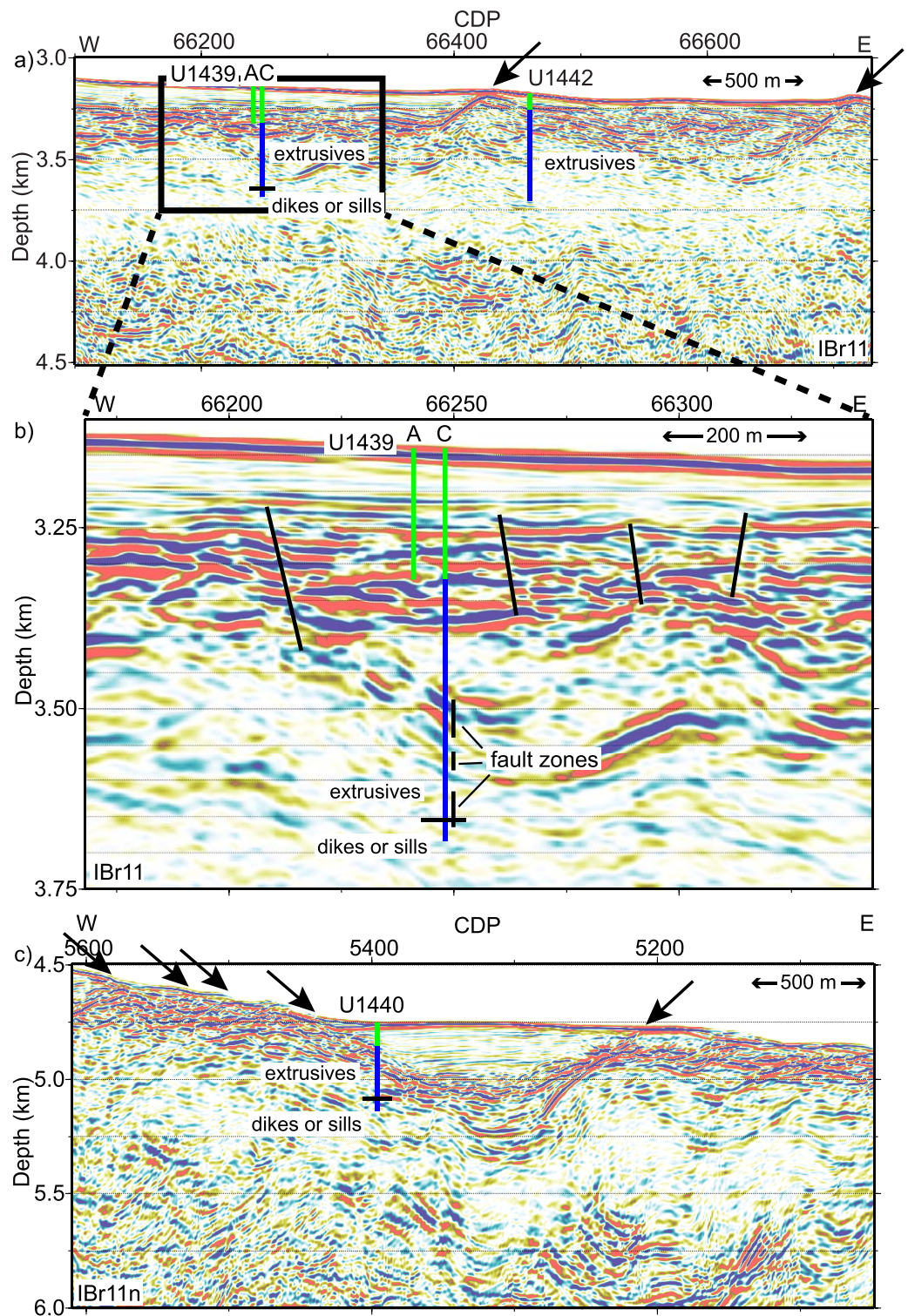
Figure 5. Prestack time migrated images, converted to depth, across Sites (a) U1439 and U1442; (b) U1439; (c) U1440. All images are plotted with a 1.0 s automatic gain control. Green lines—sediment; blue lines—basement. Arrows at seafloor mark prominent normal faults. Black lines in panel b mark interpreted high-angle faults and fault zones identified in Hole U1439C.

distance of ∼200 km (Figure 8b), while mantle refractions are sparse with no reversed coverage (Figure 8c), resulting in poorly constrained mantle velocities. The final velocity model is shown in Figure 9.
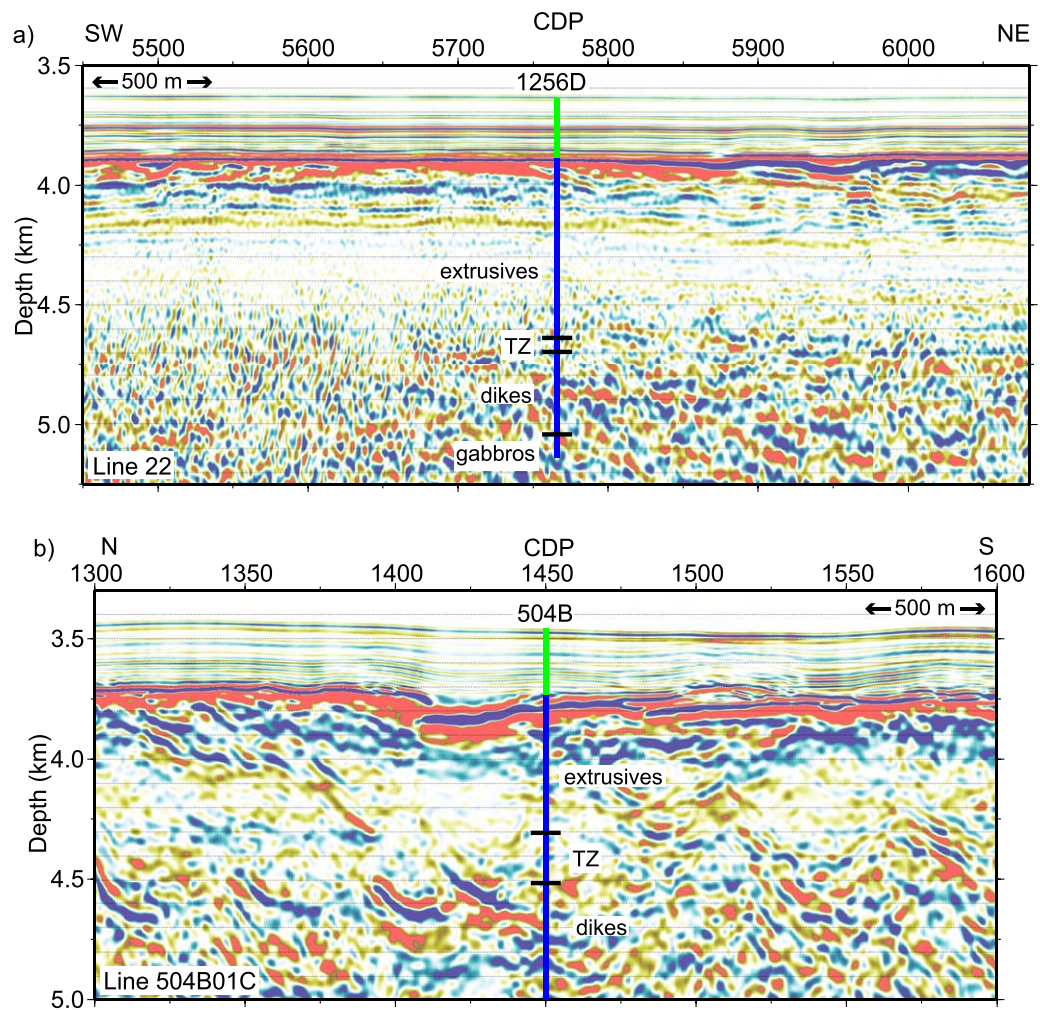
Figure 6. Prestack time migrated images, converted to depth, across Holes (a) 1256D; (b) 504B. Images are plotted with a 1.0 s automatic gain control. Green lines—sediment; blue lines—basement. TZ = transition zone.

4. Results

4.1. Discrete Sample Measurements

The Expedition 352 velocities exhibit a negative correlation with porosity (Figure 2a). There is some overlap with measurements from Holes 504B and 1256D, but in general Expedition 352 porosities are higher and have more scatter, especially for the boninite suite samples. Expedition 352 velocities exhibit a positive correlation with density (Figure 2b). Expedition 352 boninite suite samples have lower densities and more scatter than the Expedition 352 fore-arc basalts and Holes 504B and 1256D basalts, but fall close to the global relationship between velocities and densities reported by *Brocher* [2005].

4.2. Logging Measurements

P-wave sonic velocities are substantially lower for the Expedition 352 sites (mean values 3.1–3.4 km/s) compared to Holes 504B and 1256D (mean values 5.0–5.2 km/s, Figure 3a) at depths of 0–300 m below basement. Porosities are higher for the Expedition 352 sites (mean values range from 12 to 18% for the four sites) compared to Holes 504B and 1256D (mean values 8–10%), but there is some overlap especially at depths >100 m (Figure 3b). In general, densities are lower for Expedition 352 sites (mean values 2.0–2.3 g/cm^3) compared to Holes 504B and 1256D (mean values 2.5–2.6 g/cm^3), but there is some overlap for U1440B (fore-arc basalt suite) and the oceanic crust sites (Figure 3c). The gamma ray values (Figure 3d) are significantly higher for Expedition 352 sites (mean values 15–22 gAPI; see *Blum* [1997] for gAPI definition) than for oceanic crust sites (mean value 4 gAPI).
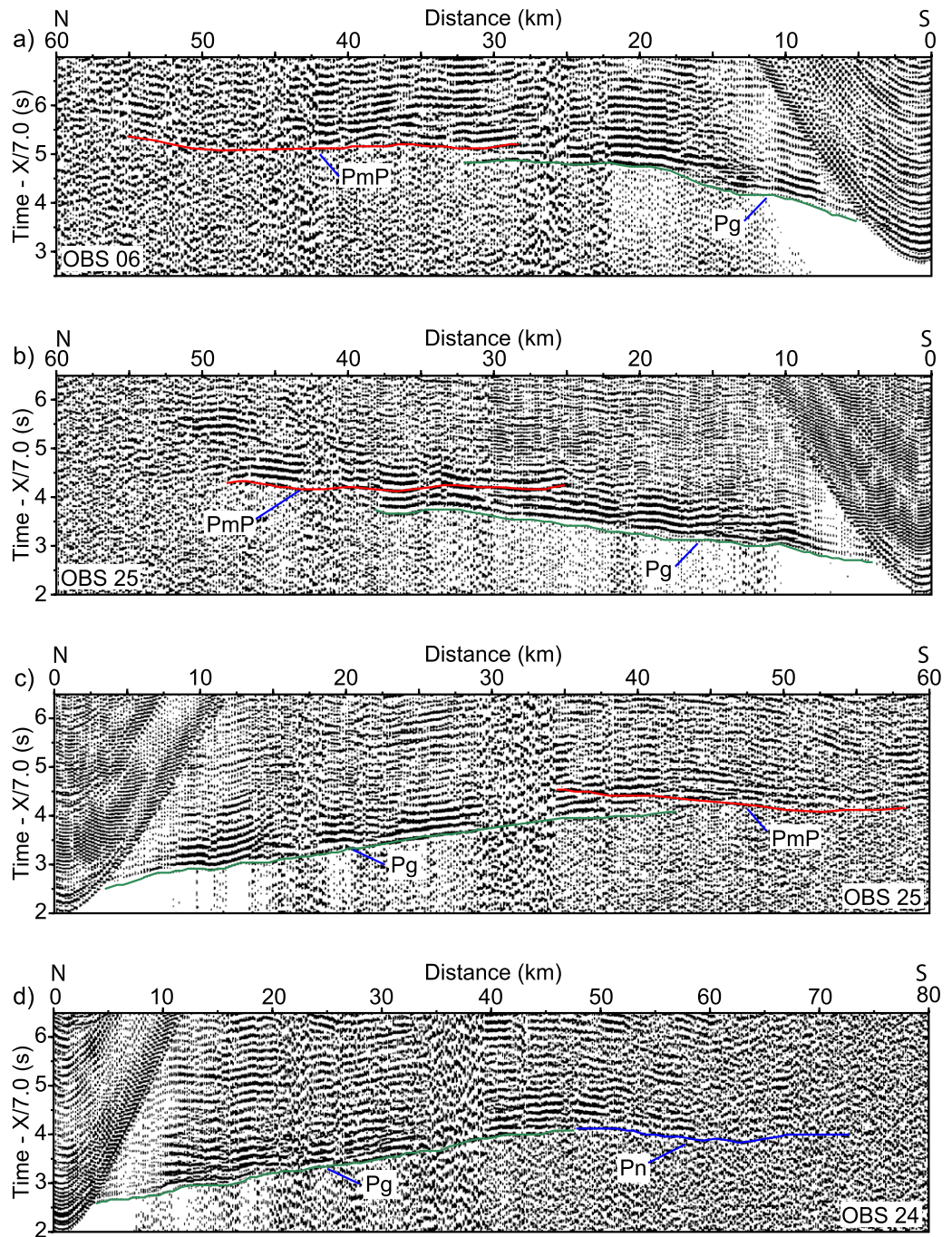
Figure 7. Representative vertical channel record sections for (a) shots north of OBS 6; (b) shots north of OBS 25; (c) shots south of OBS 25; and (d) shots south of OBS 24. Data are plotted with a reduction velocity of 7 km/s, with a 0.5 s automatic gain control applied, and with travel times picks overlain.

There is a clear separation in velocity-porosity values between Expedition 352 and Holes 504B and 1256D, with lower velocities observed for similar porosities in the IBM fore arc (Figure 4a). For velocity-density values both lower velocities and densities are observed for Expedition 352 sites compared to Holes 504B and 1256D, but all values follow the global trend between velocities and densities reported by *Brocher* [2005] (Figure 4).

Porosities in Figures 3 and 4 were not measured directly, but instead were calculated from the resistivity logs using Archie's law [*Archie*, 1942] and the method of *Becker et al.* [1982]. Alternate methods for porosity
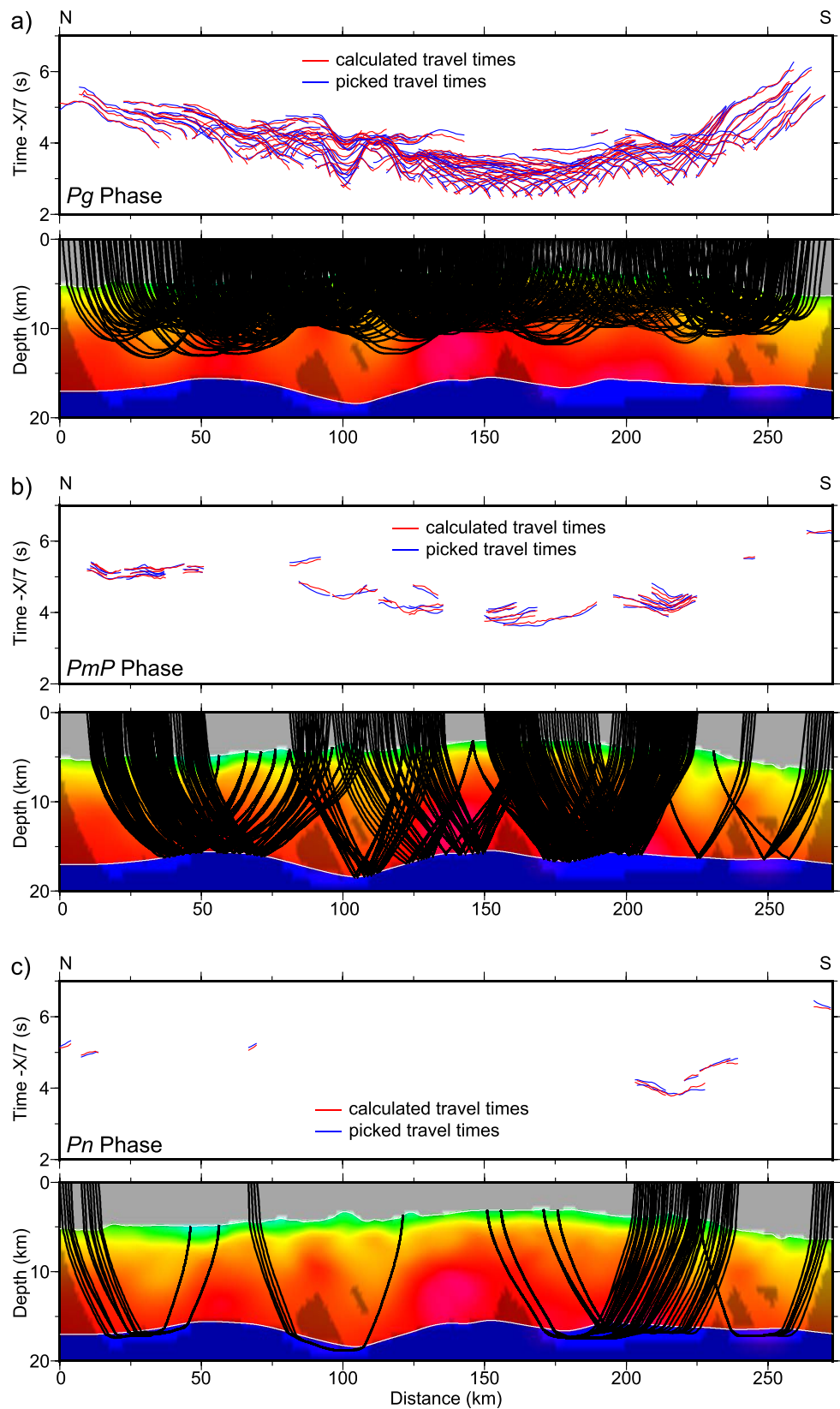
Figure 8. (a) *Pg* phase; (b) *PmP* phase; (c) *Pn* phase. (top) Comparison of observed (blue) and predicted (red) travel times plotted with a reduction velocity of 7 km/s. (bottom) Raypaths for each phase for all instruments; for *Pg* phases every fifth raypath is displayed, while all raypaths are shown for *PmP* and *Pn* phases.
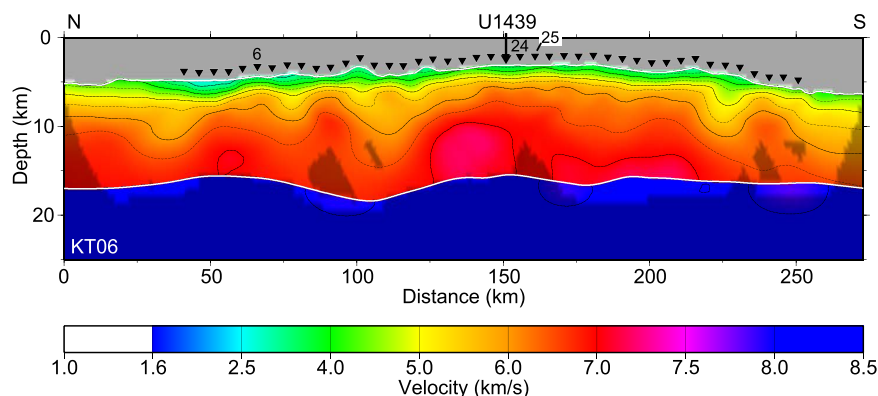
Figure 9. KT06 final velocity model, with lighter areas marking regions along profile with ray coverage. Contour interval is 0.5 km/s. White lines mark layer boundaries. Triangles plot OBS locations, with labels marking instruments with record sections plotted in Figure 7.

calculation include using different parameters in Archie's formula [*Pezard*, 1990], or calculating porosity from the density log [e.g., *Salisbury et al.*, 1989]. Both of these methods result in higher calculated porosity values, but have the same general result: lower velocities are observed for similar porosities in the IBM fore arc compared to Holes 504B and 1256D.

4.3. Crack Morphology Models

We calculate A_f values at two different scales: discrete sample and downhole logging. For discrete samples, A_f values are similar for the Expedition 352 FAB (0.088 ± 0.028), Hole 504B lavas (0.087 ± 0.031), and Hole 1256D lavas (0.061 ± 0.019), and are higher for Expedition 352 boninites (0.136 ± 0.071). Our A_f values from Hole 504B and 1256D downhole logs are 0.080 ± 0.008 and 0.074 ± 0.014, respectively (Table 1). A similar analysis by *Carlson* [2014b] for lavas at Holes 504B and 1256D found an A_f value of 0.096 ± 0.008; this slightly higher value is likely caused by the analysis of lavas at all depth ranges, while our study only included lavas at depths 25–300 m below basement. A_f values from downhole logs for the IBM region are considerably lower, with values of 0.021 ± 0.002 and 0.025 ± 0.004 for the basaltic suite and boninite suite lavas, respectively. Fits for the A_f models to the velocity-porosity discrete samples and logs are shown in Figures 2a and 4a.

4.4. Seismic Reflection Images

Normal faults, extending from the seafloor to depths of at least hundreds of meters into basement, are prevalent near all IBM sites (Figure 5). We also interpret high-angle faults in the upper 200 m of basement where layering is clearly disrupted, and dipping reflectivity is coincident with many of the fault zones identified from core samples [*Expedition 352 Scientists*, 2014] at Hole U1439C (Figure 5b). No clear faults in the upper crust are imaged within a few km of Hole 1256D (Figure 6a), but at a larger scale low-angle upper crust reflectors, with a horizontal spacing of 5–10 km, are observed on isochron profiles [*Hallenborg et al.*, 2003]. At Hole 504B some dipping reflectivity is observed (e.g., at CDPS 1375–1450, depths 4–4.75 km, Figure 6b), and normal faults are imaged at a scale larger than displayed in Figure 6b (tilted fault blocks spaced ∼10 km apart with evidence of active normal faulting [*Kent et al.*, 1996]).

4.5. Crustal Structure

Crustal thickness along IBM fore-arc profile KT06 varies from 10 to 15 km, with an average thickness of 12.3 ± 1.0 km (Figure 9). The velocity-depth function at Site U1439 is displayed in Figure 10 and consists of a high-velocity gradient upper crust with velocities increasing from ∼3.3 km/s at the seafloor to 6.0–6.2 km/s at 2.5–3.0 km depth, overlying an ∼10 km thick lower crust with velocities reaching ∼7.0 km/s at the base of the crust; upper mantle velocities are ∼8.1 km/s (Figure 10). At Hole 1256D upper Layer 2 velocities are 4.5–5 km/s, the seismic Layer 2/3 boundary is ∼1.2–1.5 km below basement, and total crustal thickness is 5–5.5 km (Figure 10) [*Expedition 309 Scientists*, 2005]. At Hole 504B velocities are 4.0–4.5 km/s near basement, the Layer 2/3 boundary is 0.9–1.2 km below basement, and total crustal thickness is ∼5 km [*Collins et al.*, 1989; *Detrick et al.*, 1994; *Swift et al.*, 1998].

5. Discussion and Conclusions

5.1. Compositional Influences
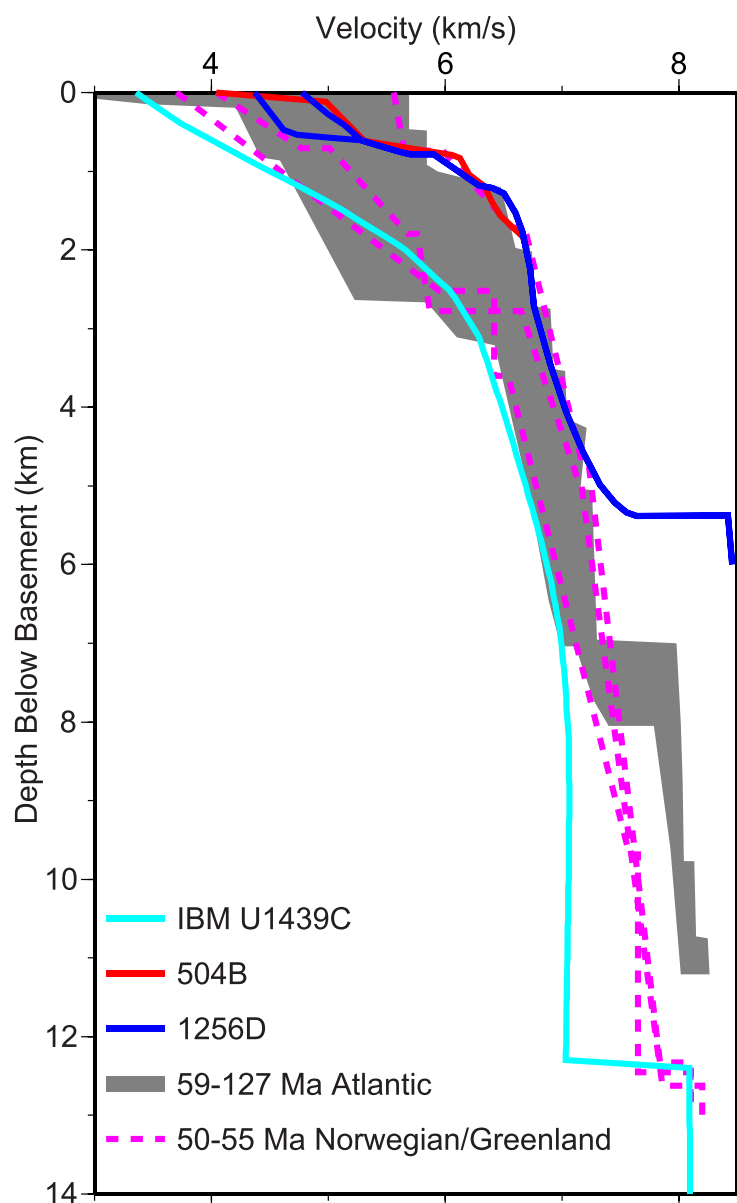
Figure 10. Comparison of velocity plotted against depth below top of basement for Site U1439 (Figure 9), Hole 1256D [*Expedition 309 Scientists*, 2005], Hole 504B [*Detrick et al.*, 1998], 59–127 Ma Atlantic oceanic crust [*White et al.*, 1992], and 50–55 Ma Norwegian and Greenland Sea thickened oceanic crust [*Mutter and Zehnder*, 1988; *Olafsson et al.*, 1992]. For Hole 1256D multiple curves are shown, as at shallow depths separate inversions were performed on northeast and southwest data subsets [*Expedition 309 Scientists*, 2005].

Before comparing IBM fore-arc crust with oceanic crust, it is important to examine effects associated with compositional differences. The basalts at Holes 504B and 1256D are N-MORB, the typical composition of oceanic crust lavas and dikes [e.g., *Alt et al.*, 1993; *Expedition 309 and 312 Scientists*, 2006]. The lavas sampled by Expedition 352 in the IBM fore arc are divided into a boninite series and a FAB series [*Reagan et al.*, 2015]. FAB is similar to N-MORB, but has lower Ti/V and Yb/V ratios indicating a depleted mantle source compared to the N-MORB source at mid-ocean ridges [*Reagan et al.*, 2010]. Boninites are high-Mg andesites with low concentrations of Ti and rare-earth elements, and high concentrations of water and fluid mobile elements, and are generated from low-pressure melting of a depleted mantle with strong fluid fluxing [e.g., *Crawford et al.*, 1989].

Figure 2 compares *P*-wave velocities, porosities, and densities for IBM fore-arc boninites, IBM fore-arc FAB, and Holes 504B and 1256D MORB discrete samples. There is considerable overlap in the MORB and FAB measurements, with slightly lower velocities and densities, and higher porosities observed for the FAB compared to MORB. The boninites exhibit a large range of measured *P*-wave velocities (3–6 km/s), densities (1.75–2.75 g/cm^3), and porosities (2–43%), but follow the same positive correlation between velocity and density, and negative correlation between velocity and porosity, as the FAB and MORB measurements (Figure 2). We use a lower grain density and grain modulus for the boninites in the A_f calculations (section 3.3), but note that the differences in these values are not statistically significant (Table 1).

Gabbros, oxide gabbros, and gabbronorites were recovered in the 100 m plutonic section at the base of Hole 1256D [*Wilson et al.*, 2006]. Noritic gabbros, which contain orthopyroxene rather than the clinopyroxene, were obtained from dredging and submersible sampling of the Bonin Ridge [*Ishizuka et al.*, 2011]. The different mineralogies are predicted to lead to densities that are ∼0.1 g/cm^3 higher for gabbronorites than gabbros, with similar *P*-wave velocities [*Abers and Hacker*, 2016].

5.2. Small-Intermediate Scale

The sonic velocity logging data indicate a clear separation in values between the IBM fore-arc and oceanic crust at Holes 504B and 1256D, with lower velocities observed at the IBM fore arc for similar depths below basement (Figure 3). There is typically an inverse relationship between velocity and porosity in oceanic crust basalts, with low velocities associated with high porosities [e.g., *Christensen et al.*, 1979; *Wilkens et al.*, 1983], but lavas with similar porosities of 9–15% have lower velocities at the IBM fore arc (2.8–3.8 km/s) than at Holes 504B and 1256D (4.0–5.2 km/s, Figure 4). Previous studies have shown that pore structure will affect the relationship between porosity and seismic velocity [e.g., *Wilkens et al.*, 1988, 1991; *Carlson*, 2014b]. For example, *Wilkens et al.* [1991] show that the closing of low-aspect ratio (flat) cracks will result in a small decrease in porosity but a large increase in seismic velocity. We use an asperity compression model [*Carlson*, 2014b] to quantify the relationship between porosities and seismic velocities for both discrete sample and logging measurements (Table 1). At the discrete sample scale, A_f values are 0.061–0.088 for Expedition 352 FAB and Holes 504B and 1256D lavas, and 0.136 for EXP boninites. A_f values from logging measurements are 0.021–0.025 for the IBM fore arc compared to values of 0.074–0.080 for oceanic crust at Holes 504B and 1256D.

A_f quantifies the fractional area of asperity contact across the cracks; smaller values signify more open (but not necessarily wider) cracks. Discrete sample *P*-wave velocity measurements are made at a frequency of 0.5 MHz, while downhole logging measurements are at frequencies of 5–15 kHz [e.g., *Reagan et al.*, 2015]; corresponding wavelengths for *P*-wave velocities of 3–5 km/s are 6–10 mm for discrete samples and 0.2–1 m for downhole logs. At the mm-scale, the discrete sample A_f values show that EXP FAB and Holes 504B and 1256D lavas have similar crack asperity populations, while EXP boninite has fewer open cracks. At the cm-m scale, the logging A_f values show a distinct difference between IBM FAB and boninites and oceanic crust, and are consistent with more open cracks in the IBM fore-arc region than for oceanic crust. Holes 504B and 1256D are located on young (6–15 Ma) intermediate-fast spreading rate crust, while the IBM fore-arc lavas are 48–52 Ma [*Ishizuka et al.*, 2011]. We therefore calculated A_f values from downhole logs at oceanic crust sites located at different ages and spreading rates to determine if the Holes 504B and 1256D A_f values are representative of oceanic crust. A_f values are 0.077, 0.062, and 0.051 for Hole 395A (slow spreading 7 Ma Atlantic crust), Hole 765D (fast spreading 154 Ma Indian crust), and Hole 801C (fast spreading 170 Ma Pacific crust), respectully. None of these A_f values approach the 0.021–0.025 A_f values observed at the IBM fore arc, indicating that neither age nor spreading rate explains the difference with values observed at Holes 504B and 1256D.

Fractured formations in oceanic crust volcanics are associated with high gamma ray values, owing to potassium-bearing secondary minerals in altered basalts [*Brewer et al.*, 1998; *Tominaga et al.*, 2009]. For example, at Hole 1256D mean gamma ray values are 5.7 gAPI for fragmented flows, compared to values of 2.6 gAPI for massive flows [*Tominaga et al.*, 2009]. In contrast, gamma ray values average 15–22 gAPI at the IBM fore-arc sites (Figure 3d). Evaluation of the IBM cores finds multiple fracturing followed by mineral precipitation from a fluid, with major vein components of calcite and various types of zeolite [*Reagan et al.*, 2015]. The potassium-rich zeolite forms from alteration of volcanic glass and is the likely source for increased gamma ray values. The 15–22 gAPI values are consistent with increased fracturing and alteration at the IBM fore arc compared to oceanic crust at Holes 504B and 1256D which have mean gamma ray values of 4 gAPI. Alteration will cause a small reduction in seismic velocity, while cracks account for the majority of the difference between in situ velocities and theoretical velocities of unaltered material [*Carlson*, 2014a].

The cracks quantified by the A_f values from downhole logs would be on the cm-m scale sampled by the logging measurements. At the larger scale, several fault zone intervals were identified in the IBM fore arc at Holes U1439C (∼348–401 mbsf, ∼420–446 mbsf, and ∼475–525 mbsf; Figure 5b) and U1442A (∼238–267 mbsf, ∼433–445 mbsf, and ∼491–502 mbsf); these fault zones are characterized by damage zones of several tens of meters in thickness, abundant slickensides, and poorly recovered cataclastic shear zones [*Reagan et al.*, 2015]. Numerous faults are imaged in seismic reflection profiles in the IBM fore arc, including normal faults extending to the seafloor and high-angle faults at 100–200 m spacing within the upper extrusive sequence (Figure 5). At Holes 504B and 1256D no fault zones are reported in the lava units [*Cann et al.*, 1983; *Wilson et al.*, 2003]. Clear faults are not imaged in MCS profiles within 1–2 km of Hole 1256D (Figure 6a), although low-angle reflectors with a horizontal spacing of 5–10 km are observed in regional profiles

[*Hallenborg et al.*, 2003]. At Hole 504B, dipping reflections are imaged that might be associated with faults (Figure 6b), and tilted fault blocks spaced ∼10 km apart, with evidence of active normal faulting, have been reported [*Kent et al.*, 1996]. Overall, faulting at Holes 504B and 1256D is not as prevalent as that imaged at the IBM fore arc (Figures 5 and 6).

5.3. Crustal Scale

The *Stern and Bloomer* [1992] model for subduction initiation of the IBM system has the earliest stages of crustal formation in a strongly extensional environment similar to spreading of slow spreading ridges, with high crustal production rates of the early arc. Typical oceanic crust has an upper crust with large velocity gradients of the order 1 s^{-1} (Layer 2) overlying a lower crust with smaller velocity gradients (Layer 3) [*White et al.*, 1992]. Layer 2 has a mean thickness of 2.1 km, with velocities of ∼2.5–6.6 km/s, while Layer 3 has a thickness of ∼5 km, with velocities typically increasing from ∼6.7 km/s at the top to ∼7.2 km/s at the base [*White et al.*, 1992]. Velocity-depth profiles from 59 to 127 Ma Atlantic oceanic crust are displayed in Figure 10 [*White et al.*, 1992]; *Kodaira et al.* [2010] argue that these provide a good comparison in respect to age and spreading rate with early seafloor generation at the IBM fore arc. Similar to oceanic crust, profile KT06 has an upper crust (Layer 2) with a large velocity gradient overlying a lower crust (Layer 3) with a smaller velocity gradient (Figures 9 and 10). The upper crust is ∼2.5–3.0 km thick and has a velocity gradient of 1.07 s^{-1} with velocities increasing from ∼3.4 to 6.2 km/s, while the lower crust is ∼9.5–10 km thick, with velocities increasing from 6.2 to 7.0 km/s at the base of the crust and a velocity gradient of ∼0.1 s^{-1} (Figures 9 and 10). Velocities at the IBM fore arc are slightly lower, and layer thicknesses are greater, than typical oceanic crust (Figure 10). Layer 2 thicknesses at Holes 504B and 1256D are 0.9–1.2 and 1.2–1.5 km, respectively, and total crustal thickness is ∼5–5.5 km at the two oceanic crust sites [*Collins et al.*, 1989; *Detrick et al.*, 1998; *Expedition 309 Scientists*, 2005]. Globally, oceanic crust has a mean thickness of 6–7 km [*Chen*, 1992; *White et al.*, 1992], which indicates that crustal thicknesses at Holes 504B and 1256D are less than average measurements, while thickness at the IBM fore arc is considerably greater.

Although oceanic crust is typically 6–7 km thick, many seismic studies have described thickened oceanic crust, where most of the crustal thickening occurs in Layer 3 [*Mutter and Mutter*, 1993]. Oceanic crust formed in the Norwegian-Greenland Sea shows variations in thickness from 7 to 20 km, with the thickest crust formed soon after initiation of seafloor spreading at 50–55 Ma [*Mutter and Mutter*, 1993]. In Figure 10 we plot the velocity structure from several Norwegian-Greenland Sea expanding spread profiles (EPSs) with crustal thickness 11–13 km [*Mutter and Zehnder*, 1988; *Olafsson et al.*, 1992]. This comparison indicates that layer thicknesses for the IBM fore-arc crust are similar to that observed for oceanic crust of comparable thickness, but that seismic velocities are lower than observed for thick oceanic crust. *Mutter and Mutter* [1993] show that average Layer 3 velocity increases with crustal thickness and argue that thicker crust with average velocities >7.1 km/s incorporates some ultramafic material. The lower velocities at the IBM fore arc, with average Layer 3 velocities of 6.9 km/s, do not require the presence of ultramafic material in the lower crust. Hydrous alteration phases, such as expected with the formation of boninite, could also be a component of the lower crust, and are consistent with Layer 3 velocities of 6.9 km/s [*Behn and Kelemen*, 2003].

Previous seismic refraction experiments near profile KT06 provide additional insights into the structure of the IBM fore arc (Figure 1). The *Kodaira et al.* [2010] Bonin ridge profile shows a significant difference between crust associated with boninitic magmatism (north half of profile) and tholeiitic-calcalkaline andesitic volcanism (south half of profile), with boninitic crust thinner with lower average crustal velocities. The KT06 profile structure is consistent with that of the northern third of the Bonin ridge profile. The *Takahashi et al.* [2009] east-west profile models four layers in this region, which they label basement (<5 km/s) and upper (∼5.9–6.2 km/s), middle (∼6.4–6.6 km/s), and lower crust (∼6.8–7.4 km/s). The basement and upper crust on the eastern edge of the Bonin ridge have total thicknesses of 2.1–4.4 km [*Takahashi et al.*, 2009], and are similar in velocity and thickness to profile KT06 2.5–3.0 km thick Layer 2. The middle and lower crust thicken beneath the Bonin ridge, with a maximum crustal thickness of 18 km [*Takahashi et al.*, 2009]; these layers are equivalent to profile KT06 Layer 3 and reveal the presence of 7.4 km/s material at the base of the crust beneath the Bonin ridge. The 10–15 km thick crust modeled along profile KT06 (Figure 9) is not representative of the entire fore arc, as *Takahashi et al.* [2009] show that total crustal thickness (from seafloor to Moho or top of subducting slab) decreases from 18 km at the Bonin ridge to 5 km near the trench.

Table 2. Mean Geophysical Observations

Parameter	IBM Fore Arc	Holes 504B and 1256D
Vp (logging), km/s	3.1–3.4	5.0–5.2
Porosity (logging), %	12–18	8–10
Density (logging), kg/m^3	2.0–2.3	2.5–2.6
Gamma ray (logging), gAPI	15–22	4
Area of contact, A_f	0.021–0.025	0.074–0.080
Imaged faults	Heavily faulted	Some faults
Layer 3 velocity, km/s	6.9	7.1
Crustal thickness, km	12.3	5–5.5

5.4. Implications and Inferences

Compared to oceanic crust, logging data at the IBM fore-arc lavas return lower compressional velocities and densities, higher porosities and gamma ray values, and lower A_f values (Table 2). Seismic profiles image many more faults at the IBM fore arc (Figure 5) than at Holes 504B and 1256D (Figure 6). As discussed in section 5.2, these observations are consistent with more fracturing and alteration at the IBM fore arc than in normal oceanic crust. At the crustal scale, IBM fore-arc crust has a layered structure similar to Holes 504B and 1256D, but total crustal thickness is significantly greater, and velocities in Layer 3 are lower than expected for thick oceanic crust (Figure 10 and Table 2). The geophysical observations summarized in Table 2 suggest that the present-day IBM fore arc is not a good analog for oceanic crust. However, it is important to consider whether the observed differences are inherent to differences in the accretionary processes at the two settings, or if initial accreted crust was similar but then subsequently modified in different ways.

Data from drill cores, borehole, and site survey data suggest that the outer IBM fore arc was deformed mainly postmagmatically [*Kurz et al.*, 2015]. Examples of this deformation include normal and strike-slip fault-bounded sedimentary basins, and tilting of the lowermost syntectonic pelagic and volcaniclastic units. At the core scale, postmagmatic deformation consists of fault zones, slickensides, shear fractures, mineralized veins, and tension fractures [*Kurz et al.*, 2015; *Reagan et al.*, 2015]. Veins formed predominantly as a consequence of hydrofracturing and as a result of extension, and cross-cutting relationships of veins point to multiple fracturing followed by mineral precipitation from a fluid [*Reagan et al.*, 2015]. Postmagmatic extension is additionally documented by extensional structures within the sedimentary sequences, especially at Sites U1439 and U1442 [*Reagan et al.*, 2015]. The prevalence of postmagmatic structures suggests that IBM fore-arc lavas, when accreted, could have had physical properties similar to that of lavas formed at a mid-ocean ridge spreading center, and then been subsequently modified by faulting and alteration owing to tectonic deformation at the IBM fore arc.

Tectonic deformation cannot explain the large differences in crustal thickness between the IBM fore arc (∼12.3 km) and Holes 504B and 1256D (∼5–5.5 km). One possibility is that thick crust was emplaced at the time of initial IBM fore-arc spreading; however, if so, it has unusually low Layer 3 seismic velocities compared to other studies of thick oceanic crust. For example, the 11.5–13 km thick Norwegian and Greenland Sea oceanic crust shown in Figure 10 has an average Layer 3 velocity of ∼7.3 km/s, which is interpreted to incorporate some ultramafic material [*Mutter and Zehnder*, 1988; *Olafsson et al.*, 1992; *Mutter and Mutter*, 1993]. Thicker crust to the west under the Bonin ridge does have velocities of 7.4 km/s at the base of the crust [*Takahashi et al.*, 2009], and it is possible that ultramafic material is localized to this region.

Alternatively, crust at the IBM fore arc could have been thickened after emplacement. Initial spreading near the Bonin Ridge emplaced fore-arc lavas ∼50–52 Ma, and later volcanism evolved to boninites (∼46–48 Ma) and andesites (41–44 Ma) [*Stern and Bloomer*, 1992; *Ishizuka et al.*, 2011; *Reagan et al.*, 2013]. Magmatic activity appears to retreat from the trench, with the fore-arc lavas found at sites U1440 and U1441 and in submersible dives close to the trench, boninites found at sites U1439 and U1442 and on the Bonin ridge, and andesites on the western portion of the Bonin ridge (Figure 1) [*Reagan et al.*, 2010; *Ishizuka et al.*, 2011; *Reagan et al.*, 2015]. Despite differences in lava composition, crustal structure is continuous for fore-arc crust from the Bonin ridge to the trench, with changes in thickness but only minor changes in velocity [*Takahashi et al.*, 2009]. *Ishizuka et al.* [2006] argue that a broad swath (∼150–200 km in their generalized cross section) of fore-arc crust formed by seafloor spreading with boninitic volcanism after subduction initiation, and was later the location of andesitic volcanism that retreated from the trench to the Bonin Ridge. *Ishizuka et al.* [2011] have a variation on this model, with initial FAB volcanism forming oceanic crust in the fore arc, which is overlain by boninitic and later arc lavas. Both of these models suggest that there is not a simple progression with time of magmatism away from the trench but that magmatism is over a broad region that includes the crust formed from initial spreading. Thickening of the crust could occur through continued

magmatism, prior to evolution to mature subduction and the present-day arc. At sites U1439 and U1442 thrust faults are observed in the cores that predate extensional structures, so part of the crustal thickening might also be related to early thrusting [*Reagan et al.*, 2015]. The second model is consistent with the recovery of FAB in the IBM back arc during IODP Expedition 351 [*Arculus et al.*, 2015]. FAB could have been emplaced over an extensive region from near the trench to the present-day back arc, followed by localized emplacement near the Bonin ridge of boninites.

Our study has focused on a comparison between the IBM fore-arc and oceanic crust, but we can also compare some physical properties directly with ophiolites. However, when doing so we need to consider that some physical properties may have changed during and after emplacement on land. In Figure 2 we plot velocity, density, and porosity values for Semail ophiolite basalts [*Christensen and Smewing*, 1981] and Bay of Islands (BOI) ophiolite metabasalts [*Salisbury and Christensen*, 1978; *Christensen and Salisbury*, 1982]. The velocity measurements were made at pressures of 0.06–0.08 GPa; 0.18 km/s [*Christensen*, 1972] has been subtracted from the velocity values for comparison with the other samples which were measured at ambient pressure. Porosity values are only reported for the BOI metabasalts; these are low compared to oceanic crust and the IBM fore arc, but the porosity reduction likely occurred during the change from basalts to metabasalts. Velocities and densities of the ophiolite basalts, ophiolite metabasalts, ocean crust basalts, and Expedition 352 FAB all follow the same velocity-density trends (but have higher densities than the Expedition 352 boninites).

In Figure 3 we include average formation properties derived from logs in the Troodos ophiolite [*Salisbury et al.*, 1989]. P-wave velocities for the Troodos ophiolite pillow basalts are ∼3.2–3.4 km/s at depths <300 m and are remarkably similar to the 3.1–3.4 km/s mean values measured at the Expedition 352 sites. Porosity values are estimated at ∼23%; porosities are calculated from the density log and might not be directly comparable to the values calculated from the resistivity logs for the Expedition 352 and ocean crust sites. Density values for the Troodos ophiolite basalts average 2.25 g/cm^3 at depths <300 m, which are comparable to the 2.0–2.3 g/cm^3 mean values measured at the Expedition 352 sites, and less than the 2.5–2.6 g/cm^3 mean values measured at Holes 504B and 1256D. Gamma ray values of 22–29 API for the Troodos ophiolite basalts in Figure 3d are slightly higher than the 15–22 gAPI values of the Expedition 352 sites and much higher than the 4 gAPI mean value measured at Holes 504B and 1256D. Overall, the velocity-porosity, velocity-density, and gamma ray values of the Troodos ophiolite are closer to the IBM fore-arc measurements than the oceanic crust measurements (Figures 3 and 4).

The IBM fore-arc seismic refraction profile modeled velocities that are slightly lower, and layer thicknesses that are greater, than typical oceanic crust (Figures 9 and 10). The IANGASS seismic refraction profile across the Troodos ophiolite modeled a ∼1.5 km thick upper layer with velocities ∼2.5–5.0 km/s, underlain by a ∼4–4.5 km thick layer with velocities ∼6.0–6.7 km/s, which is underlain by a ∼6 km thick layer with velocities of 6.9–7.1 km/s [*Mackenzie et al.*, 2006]. *Mackenzie et al.* [2006] present two hypotheses for the 6 km thick ∼7 km/s layer: partially serpentinized peridotite or ultramafic cumulates. If the basal layer is serpentinized mantle, then the Troodos crust is ∼5 km thick, whereas if it is composed of ultramafic cumulates, then the crust is ∼11 km thick. Although *Mackenzie et al.* [2006] prefer an interpretation of ∼5 km thick crust underlain by serpentinized mantle, we note that 11 km thick crust with basal velocities of ∼7 km/s compares well with the IBM fore-arc KT06 profile with 12.5 km thick crust and similar basal velocities.

What are the implications for using SSZ crust as an analog for ophiolites, and ophiolites as an analog for oceanic crust? At the cm-m scale (discrete sample), physical properties of lavas follow similar trends, suggesting that there are no inherent differences owing to emplacement at different tectonic settings. However, these lavas were either emplaced in thick crust, or the crust was thickened through continued magmatism after initial accretion following subduction initiation. Subsequently, the crust was modified by faulting and alteration owing to tectonic deformation at the IBM fore arc. Hence, crust composing ophiolites formed at SSZ settings could be modified after accretion and before obduction; these processes should be considered when using ophiolites as an analog for oceanic crust.

References

Abers, G. A., and B. R. Hacker (2016), A MATLAB toolbox and Excel workbook for calculating the densities, seismic wave speeds, and major element composition of minerals and rocks at pressure and temperature, *Geochem. Geophys. Geosyst.*, *17*, 616–624, doi:10.1002/2015GC006171.

Alt, J. C., H. Kinoshita, L. B. Stokking, and ODP Leg 148 Shipboard Party (1993), *Proceedings of Ocean Drilling Program Initial Reports*, vol. 148, Ocean Drill. Program, College Station, Tex.

Anderson, R. N., et al. (1982), DSDP Hole 504B, the first reference section over 1 km through Layer 2 of the oceanic crust, *Nature*, *300*, 589–594.

Anonymous (1972), Penrose field conference report, *Geotimes*, *17*, 24–25.

Archie, G. E. (1942), The electrical resistivity log as an aid in determining some reservoir characteristics, *Trans. AIME*, *146*, 54–62.

Arculus, R. J., et al. (2015), A record of spontaneous subduction initiation in the Izu-Bonin-Mariana arc, *Nat. Geosci.*, *8*, 728–733, doi:10.1038/ngeo2515.

Becker, K., et al. (1982), In situ electrical resistivity and bulk porosity of the oceanic crust Costa Rica Rift, *Nature*, *300*, 594–598.

Becker, K., et al. (1989), Drilling deep into young oceanic crust, Hole 504B, Costa Rica Rift, *Rev. Geophys.*, *27*, 79–102.

Behn, M. D., and P. B. Kelemen (2003), Relationship between seismic P-wave velocity and the composition of anhydrous igneous and meta-igneous rocks, *Geochem. Geophys. Geosyst.*, *4*(5), 1041, doi:10.1029/2002GC000393.

Blum, P. (1997), *Physical Properties Handbook: A Guide to the Shipboard Measurement of Physical Properties of Deep-Sea Cores, Tech. Note 26*, Ocean Drill. Program, College Station, Tex., doi:10.2973/odp.tn.26.1997.

Brewer, T. S., P. K. Harvey, M. A. Lovell, S. Haggas, G. Williamson, and P. Pezard (1998), Ocean floor volcanism: Constraints from the integration of core and downhole logging measurements, *Geol. Soc. Spec. Publ.*, *136*, 341–362, doi:10.1144/gsl.sp.1998.136.01.28.

Brocher, T. M. (2005), Empirical relations between elastic wavespeeds and density in the Earth's crust, *Bull. Seismol. Soc. Am.*, *95*, 2081–2092, doi:10.1785/0120050077.

Cann, J. R., M. G. Langseth, J. Honnorez, R. P. Von Herzon, S. M. White, and Shipboard Scientific Party (1983), *Deep Sea Drilling Project Initial Reports*, vols. 69–70, U.S. Gov. Print. Off., Washington, D. C.

Carlson, R. L. (2014a), The effects of alteration and porosity on seismic velocities in oceanic basalts and diabases, *Geochem. Geophys. Geosyst.*, *15*, 4589–4598, doi:10.1002/2014GC005537.

Carlson, R. L. (2014b), The influence of porosity and crack morphology on seismic velocity and permeability in the upper oceanic crust, *Geochem. Geophys. Geosyst.*, *15*, 10–27, doi:10.1002/2013GC004965.

Chen, Y. J. (1992), Oceanic crustal thickness versus spreading rate, *Geophys. Res. Lett.*, *19*, 753–756.

Christensen, N. I. (1972), Compressional and shear wave velocities at pressures to 10 kilobars for basalts from the East Pacific Rise, *Geophys. J. R. Astron. Soc.*, *28*, 425–429.

Christensen, N. I., and M. H. Salisbury (1982), Lateral heterogeneity in the seismic structure of the oceanic crust inferred from velocity studies in the Bay of Islands ophiolite, Newfoundland, *Geophys. J. R. Astron. Soc.*, *68*, 675–688.

Christensen, N. I., and J. D. Smewing (1981), Geology and seismic structure of the northern section of the Oman ophiolite, *J. Geophys. Res.*, *86*, 2545–2555.

Christensen, N. I., S. C. Blair, R. H. Wilkens, and M. H. Salisbury (1979), Compressional wave velocities, densities, and porosities of basalts from Holes 417A, 417D, and 418A, in *Deep Sea Drilling Project Initial Reports*, vol. 51–53, edited by T. W. Donnelly et al., pp. 1467–1472, U.S. Gov. Print. Off., Washington, D. C., doi:10.2973/dsdp.proc.515253.1980.

Christeson, G. L. (2016a), Reprocessed multichannel seismic data across ODP Site 504B in the eastern Pacific Ocean, acquired in 1994 during the R/V Marcus Ewing survey EW9416, Academic Seismic Portal at UTIG, *Mar. Geosci. Data Syst.*, doi:10.1594/IEDA/500070.

Christeson, G. L. (2016b), Reprocessed multichannel seismic data across ODP Site 1256D in the eastern Pacific Ocean, acquired in 1999 during the R/V Marcus Ewing survey EW9903, Academic Seismic Portal at UTIG, *Mar. Geosci. Data Syst.*, doi:10.1594/IEDA/500071.

Collins, J. A., G. M. Purdy, and T. M. Brocher (1989), Seismic velocity structure at Deep Sea Drilling Project site 504B, Panama Basin: Evidence for thin oceanic crust, *J. Geophys. Res.*, *94*, 9283–9302.

Crawford, A. J., T. J. Falloon, and D. H. Green (1989), Classification, petrogensis and tectonic setting of boninites, in *Boninites and Related Rocks*, edited by A. J. Crawford, pp. 1–49, Unwin Hyman, London.

Detrick, R., J. Collins, R. Stephen, and S. Swift (1994), In situ evidence for the nature of the seismic layer 2/3 boundary in oceanic crust, *Nature*, *370*, 288–290.

Detrick, R. S., D. R. Toomey, and J. A. Collins (1998), Three-dimensional upper crustal heterogeneity and anisotropy around Hole 504B from seismic tomography, *J. Geophys. Res.*, *103*, 30,485–30,504.

Expedition 309 and 312 Scientists (2006), Superfast spreading rate crust 3: A complete in situ section of upper oceanic crust formed at a superfast spreading rate, *Prelim. Rep. Integrated Ocean Drill. Program*, *312*, 1–168, doi:10:2204/iodp.pr.312.2006.

Expedition 309 Scientists (2005), Superfast spreading rate crust 2: A complete in situ section of upper oceanic crust formed at a superfast spreading rate, *Prelim. Rep. Integrated Ocean Drill. Program*, *309*, 1–128, doi:10:2204/iodp.pr.309.2005.

Expedition 335 Scientists (2011), Superfast spreading rate crust 4: Drilling gabbro in intact ocean crust formed at a superfast spreading rate, *Prelim. Rep. Integrated Ocean Drill. Program*, *335*, 1–149, doi:10.2204/iodp.pr.335.2011.

Expedition 352 Scientists (2014), Izu-Bonin-Mariana fore arc: Testing subduction initiation and ophiolite models by drilling the outer Izu-Bonin-Mariana fore arc, *Prelim. Rep. Integrated Ocean Drill. Program*, *352*, 1–35, doi:10.14379/iodp.pr.352.2014.

Guerin, G., D. S. Goldberg, and G. J. Iturrino (2008), Velocity and attenuation in young oceanic crust: New downhole log results from DSDP/ODP/IODP Holes 504B and 1256D, *Geochem. Geophys. Geosyst.*, *9*, Q12014, doi:10.1029/2008GC002203.

Hallenborg, E., A. J. Harding, G. M. Kent, and D. S. Wilson (2003), Seismic structure of 15 Ma oceanic crust formed at an ultrafast spreading East Pacific Rise: Evidence for kilometer-scale fracturing from dipping reflectors, *J. Geophys. Res.*, *108*(B11), 2532, doi:10.1029/2003JB002400.

Hilde, T. W. C., S. Uyeda, and L. Kroenke (1977), Evolution of the western pacific and its margin, *Tectonophysics*, *38*, 145–165, doi:10.1016/0040-1951(77)90205-0.

Ishizuka, O., et al. (2006), Early stages in the evolution of Izu–Bonin arc volcanism: New age, chemical, and isotopic constraints, *Earth Planet. Sci. Lett.*, *250*, 385–401, doi:10.1016/j.epsl.2006.08.007.

Ishizuka, O., K. Tani, M. K. Reagan, K. Kanayama, S. Umino, Y. Harigane, I. Sakamoto, Y. Miyajima, M. Yuasa, and D. J. Dunkley (2011), The timescales of subduction initiation and subsequent evolution of an oceanic island arc, *Earth Planet. Sci. Lett.*, *306*, 229–240.

Karato, S., R. H. Wilkens, and M. G. Langseth (1983), Shipboard physical-properties measurements of basalts from the Costa Rica Rift, in *Deep Sea Drilling Project Initial Reports*, vol. 69, edited by J. Cann et al., U.S. Gov. Print. Off., Washington, D. C.

Kent, G. M., S. A. Swift, R. S. Detrick, J. A. Collins, and R. A. Stephen (1996), Evidence for active normal faulting on 5.9 Ma crust near Hole 504B on the southern flank of the Costa Rica rift, *Geology*, *24*, 83–86, doi:10.1130/0091-7613(1996)024<0083:efanfo>2.3.co;2.

Kent, G. M., R. S. Detrick, S. A. Swift, J. A. Collins, and I. I. Kim (1997), Evidence from Hole 504B for the origin of dipping events in oceanic crustal reflection profiles as out-of-plane scattering from basement topography, *Geology*, *25*, 131–134.

Kodaira, S., N. Noguchi, N. Takahashi, O. Ishizuka, and Y. Kaneda (2010), Evolution from fore-arc oceanic crust to island arc crust: A seismic study along the Izu-Bonin fore arc, *J. Geophys. Res.*, *115*, B09201, doi:10.1029/2009JB006968.

Kurz, W., E. C. Ferre, A. H. F. Robertson, A. J. Avery, S. Kutterolf, and IODP Expedition 352 Scientists (2015), Tectonic evolution of the outer Izu-Bonin-Mariana fore arc system: Initial results from IODP Expedition 352, Abstract T32C-07 presented at 2010 Fall Meeting, AGU, San Francisco, Calif., 14–18 Dec.

Mackenzie, G. D., P. K. H. Maguire, L. A. Coogan, M. A. Khan, M. Eaton, and G. Petrides (2006), Geophysical constraints on the crustal architecture of the Troodos ophiolite: Results from the IANGASS project, *Geophys. J. Int.*, *167*, 1385–1401.

Miyashiro, A. (1973), The Troodos ophiolitic complex was probably formed in an island arc, *Earth Planet. Sci. Lett.*, *19*, 218–224, doi:10.1016/0012-821X(73)90118-0.

Moores, E. M., and F. J. Vine (1971), The Troodos Massif, Cyprus and other ophiolites as oceanic crust: Evaluation and implications, *Philos. Trans. R. Soc. London A*, *268*, 443–466.

Mutter, C. Z., and J. C. Mutter (1993), Variations in thickness of layer 3 dominate oceanic crustal structure, *Earth Planet. Sci. Lett.*, *117*, 295–317.

Mutter, J. C., and C. M. Zehnder (1988), Deep crustal structure and magmatic processes: The inception of seafloor spreading in the Norwegian-Greenland Sea, *Geol. Soc. Spec. Publ.*, *39*, 35–48, doi:10.1144/gsl.sp.1988.039.01.05.

Olafsson, I., E. Sundvor, O. Eldholm, and K. Grue (1992), Møre Margin: Crustal structure from analysis of expanded spread profiles, *Mar. Geophys. Res.*, *14*, 137–162.

Pearce, J. A., S. J. Lippard, and S. Roberts (1984), Characteristics and tectonic significance of supra-subduction zone ophiolites, *Geol. Soc. Spec. Publ.*, *16*, 77–94, doi:10.1144/gsl.sp.1984.016.01.06.

Pezard, P. A. (1990), Electrical properties of mid-ocean ridge basalt and implications for the structure of the upper oceanic crust in Hole 504B, *J. Geophys. Res.*, *95*, 9237–9264.

Reagan, M. K., O. Ishizuka, R. J. Stern, K. A. Kelley, Y. Ohara, J. Blichert-Toft, S. H. Bloomer, J. Cash, P. Fryer, and B. B. Hanan (2010), Fore-arc basalts and subduction initiation in the Izu-Bonin-Mariana system, *Geochem. Geophys. Geosyst.*, *11*, Q03X12, doi:10.1029/2009GC002871.

Reagan, M. K., W. C. McClelland, G. Girard, K. R. Goff, D. W. Peate, Y. Ohara, and R. J. Stern (2013), The geology of the southern Mariana fore-arc crust: Implications for the scale of Eocene volcanism in the western Pacific, *Earth Planet. Sci. Lett.*, *380*, 41–51.

Reagan, M. K., J. A. Pearce, K. Petronotis, and Expedition 352 Scientists (2015), Izu-Bonin-Mariana fore arc, in *Proceedings of the International Ocean Discovery Program*, vol. 352, Int. Ocean Discovery Program, College Station, Tex., doi:10.14379/iodp.proc.352.2015.

Ryan, W. B. F., et al. (2009), Global multi-resolution topography synthesis, *Geochem. Geophys. Geosyst.*, *10*, Q03014, doi:10.1029/2008GC002332.

Salisbury, M. H., and N. I. Christensen (1978), The seismic velocity structure of a traverse through the Bay of Islands ophiolite complex, Newfoundland: An exposure of oceanic crust and upper mantle, *J. Geophys. Res.*, *83*, 805–817.

Salisbury, M. H., N. I. Christensen, F. J. Vine, G. C. Smith, and S. Eleftheriou (1989), Geophysical structure of the Troodos ophiolite from downhole logging, in *Cyprus Crustal Study Project: Initial Report, Hole CY-4*, vol. 88-9, edited by I. L. Gibson, et al., pp. 331–349, Geol. Soc. of Can., Waterloo, Ontario.

Shipboard Scientific Party (2003), Site 1256, in *Proceedings of the Ocean Drilling Program Initial Reports*, vol. 206, edited by D. S. Wilson, et al., pp. 1–396, Ocean Drill. Program, College Station, Tex., doi:10.2973/odp.proc.ir.206.103.2003.

Stern, R. J., and S. H. Bloomer (1992), Subduction zone infancy: Examples from the Eocene Izu-Bonin-Mariana and Jurassic California arcs, *Geol. Soc. Am. Bull.*, *104*, 1621–1636, doi:10.1130/0016-7606(1992)104<1621:szieft>2.3.co;2.

Swift, S. A., D. Lizarralde, R. A. Stephen, and H. Hoskins (1998), Velocity structure in upper ocean crust at Hole 504B from vertical seismic profiles, *J. Geophys. Res.*, *103*, 15,361–15,376.

Takahashi, N., S. Kodaira, Y. Tatsumi, M. Yamashita, T. Sato, Y. Kaiho, S. Miura, T. No, K. Takizawa, and Y. Kaneda (2009), Structural variations of arc crusts and rifted margins in the southern Izu-Ogasawara arc–back arc system, *Geochem. Geophys. Geosyst.*, *10*, Q09X08, doi:10.1029/2008GC002146.

Tominaga, M., D. A. H. Teagle, J. C. Alt, and S. Umino (2009), Determination of the volcanostratigraphy of oceanic crust formed at superfast spreading ridge: Electrofacies analyses of ODP/IODP Hole 1256D, *Geochem. Geophys. Geosyst.*, *10*, Q01003, doi:10.1029/2008GC002143.

Van Avendonk, H. J. A., D. J. Shillington, W. S. Holbrook, and M. J. Hornbach (2004), Inferring crustal structure in the Aleutian island arc from a sparse wide-angle seismic data set, *Geochem. Geophys. Geosyst.*, *5*, Q08008, doi:10.1029/2003GC000664.

White, R. S., D. McKenzie, and K. O'Nions (1992), Oceanic crustal thickness from seismic measurements and rare earth element inversions, *J. Geophys. Res.*, *97*, 19,683–19,715, doi:10.1029/92JB01749.

Wilkens, R. H., G. J. Fryer, and J. Karsten (1991), Evolution of porosity and seismic structure of upper oceanic crust: Importance of aspect ratios, *J. Geophys. Res.*, *96*, 17,981–17,995.

Wilkens, R. H., N. I. Christensen, and L. Slater (1983), High pressure seismic studies of Leg 69 and 70 basalts, in *Deep Sea Drilling Project Initial Reports*, vol. 69, edited by J. R. Cann, et al., pp. 683–686, U.S. Govt. Printing Office, Washington, D. C., doi:10.2973/dsdp.proc.69.142.1983.

Wilkens, R. H., D. Schultz, and R. L. Carlson (1988), Relationship of resistivity, velocity, and porosity for basalts from downhole well-logging measurements in Hole 418A, in *Proceedings of Ocean Drilling Program Scientific Results*, vol. 102, edited by M. H. Salisbury, et al., pp. 69–75, Ocean Drill. Program, College Station, Tex., doi:10.2973/odp.proc.sr.102.119.1988.

Wilson, D. S., D. A. H. Teagle, G. D. Acton, and Leg 206 Science Party (2003), *Proceedings of Ocean Drilling Program Initial Reports*, vol. 206, 396 pp., Ocean Drill. Program, College Station, Tex.

Wilson, D. S., et al. (2006), Drilling to Gabbro in intact ocean crust, *Science*, *312*, 1016–1020, doi:10.1126/science.1126090.